

Zhenpei Yang^{1,*} Zhile Ren² Qi Shan² Qixing Huang¹
¹The University of Texas at Austin ²Apple

Abstract

Deep learning has made significant impacts on multi-view stereo systems. State-of-the-art approaches typically involve building a cost volume, followed by multiple 3D convolution operations to recover the input image’s pixel-wise depth. While such end-to-end learning of plane-sweeping stereo advances public benchmarks’ accuracy, they are typically very slow to compute. We present MVS2D, a highly efficient multi-view stereo algorithm that seamlessly integrates multi-view constraints into single-view networks via an attention mechanism. Since MVS2D only builds on 2D convolutions, it is at least 4× faster than all the notable counterparts. Moreover, our algorithm produces precise depth estimations, achieving state-of-the-art results on challenging benchmarks ScanNet, SUN3D, and RGBD. Even under inexact camera poses, our algorithm still out-performs all other algorithms. Supplementary materials and code will be available at the project page: <https://zhenpeiyang.github.io/MVS2D>

1. Introduction

Multi-view Stereo (MVS) aims to reconstruct the underlying 3D scene or estimate the dense depth map using multiple neighboring views. It plays a key role in a variety of 3D vision tasks. With high-quality cameras becoming more and more accessible, there are growing interests in developing reliable and efficient stereo algorithms in various applications, such as 3D reconstruction, augmented reality, and autonomous driving. As a fundamental problem in computer vision, MVS has been extensively studied [7]. Recent research shows that deep neural networks, especially convolutional neural networks (CNNs), lead to more accurate and robust systems than traditional solutions. Several approaches [15, 45] report exceptional accuracy on challenging benchmarks like ScanNet [5] and SUN3D [37].

State-of-the-art CNN-based multi-view approaches typically fall into three categories: 1) Variants of a standard 2D UNet architecture with feature correlation [20, 17]. However, these approaches work best for rectified stereo pairs,

* Experiments are conducted by Z. Yang at The University of Texas at Austin. Email: yzp@utexas.edu

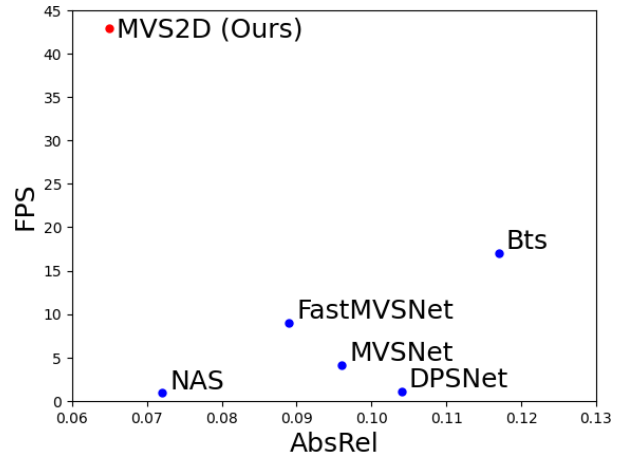


Figure 1: Inference frame per second (FPS) vs. depth error (AbsRel) on ScanNet [5]. Our model achieve significant reduction in inference time, while maintaining state-of-the-art accuracy.

and extending them to multi-view is nontrivial. 2) Constructing a differential 3D cost volume [11, 12, 41, 22, 42, 9]. These algorithms significantly improve the accuracy of MVS, but at the cost of heavy computational burdens. Furthermore, the predicted depth map by 3D convolution usually contains salient artifacts which have to be rectified by a 2D refinement network [12]. 3) Maintain a global scene representation and fuse multi-view information through ray-casting features from 2D images [21]. This paradigm cannot handle large-scale scenes because of the vast memory consumption on maintaining a global representation.

Aside from multi-view depth estimation, we have also witnessed the tremendous growth of single-view depth prediction networks [16, 44, 38, 24, 40]. As shown in Table 2, Bts [16] has achieved impressive result on ScanNet [5]. Single-view depth prediction roots in learning feature representations to capture image semantics, which is orthogonal to correspondence-computation in multi-view techniques. A natural question is how to combine single-view depth cues and multi-view depth cues.

We introduce MVS2D that combines the strength of single-view and multi-view depth estimations. The core contribution is an attention mechanism that aggregates features along epipolar lines of each query pixel on the refer-

ence images. This module captures rich signals from the reference images. Most importantly, it can be easily integrated into standard CNN architectures defined on the input image, introducing relatively low computational cost.

Our attention mechanism possesses two appealing characteristics: 1) Our network only contains 2D convolutions. 2) Besides relying on the expressive power of 2D CNNs, the network seamlessly integrates single-view feature representations and multi-view feature representations. Consequently, MVS2D is the most efficient approach compared to state-of-the-art algorithms (See Figure 1). It is $48\times$ faster than NAS [15], $39\times$ faster than DPSNet [12], $10\times$ faster than MVSNet [41], and more than $4\times$ speed-up over the previous fastest approach FastMVSNet [45]. In the meantime, MVS2D achieves state-of-the-art accuracy.

Intuitively, the benefit of MVS2D comes from the early fusion of the intermediate feature representations. The outcome is that the intermediate feature representations contain rich 3D signals, which can promote the attention module’s performance, i.e., on finding better correspondences. Moreover, instead of merely focusing on the source image’s depth cues, our approach also aggregates single-view depth cues of the reference images through the learned feature representations. Furthermore, MVS2D offers ample space where we can design locations of the attention modules to address different inputs.

One example is when the input camera poses are inaccurate, and corresponding pixels deviate from the epipolar lines on the input reference images. We demonstrate a simple solution, which installs multi-scale attention modules on an encoder-decoder network. In this configuration, corresponding pixels in down-sampled reference images lie on the epipolar lines, and MVS2D detect and rectify correspondences automatically.

We conduct extensive experiments on challenging benchmarks ScanNet [5], SUN3D [37], RGBD [28] and Scenes11 [28]. MVS2D achieves the state-of-the-art performance on nearly all the metrics. Qualitatively, compared to recent approaches [12, 41, 15, 45], MVS2D helps generate higher quality 3D reconstruction outputs.

2. Related Works

Recent advances of multi-view stereo. Multi-view stereo algorithms can be categorized into depth map-based approaches, where the output is a per-view depth map, or point-based approaches, where the output is a sparse reconstruction of the underlying scene (cf. [7]). Many traditional multi-view stereo algorithms follow a match-then-reconstruct paradigm [8] that leverages the sparse-nature of feature correspondences. Such a paradigm typically fails to reconstruct textureless regions where correspondences are not well-defined. Along this line, Zbontar *et al.* [46] provided one of the first attempts to bring the power of feature learning into multi-view stereo. They proposed a su-

pervised feature learning approach to find the correspondences. Recently, researchers have found that depth map-based approaches [13, 11, 41, 12, 42] are more favorable than those that follow the match-and-reconstruct paradigm. A key advantage of these approaches is that they can utilize the efficiency of regular tensor operations. [41, 12] proposed an end-to-end plane-sweeping stereo approach that constructs learnable 3D cost volume. While MVSNet [41] focuses on the reconstruction of 3D scene, DPSNet [12] focuses on evaluating the per-view depth-map accuracy. Researchers have also explored other 3D representations to regularized the prediction, such as point clouds [3], surface normals [15], or meshes [36]. There are also several benchmark datasets for this task [43, 37, 28, 1, 5, 33].

Cost volume for multi-view stereo. A recent line of works on multi-view stereo utilizes the notion of *cost volume*, which contains feature matching costs for a pair of images [10]. This feature representation has been successfully implemented in various pixel-wise matching tasks like optical flow [29]. Authors of MVSNet [41] and DPSNet [12] proposed to first construct a differentiable cost volume and then use the power of 3D CNNs to regularize the cost volume before predicting per-pixel depth or disparity. Most recent state-of-the-art approaches follow such a paradigm [42, 22, 9, 3, 45, 18]. However, the size of the cost volume ($C \times K \times H \times W$) is linearly related to the number of depth hypotheses K . These approaches are typically slow in both training and inference. For example, DPSNet [12] takes several days to train on ScanNet; NAS [15] takes even longer because of its extra training of a depth-normal consistency module. Recently, Murez *et al.* [21] proposed to construct a volumetric scene representation from a calibrated image sequence for scene reconstruction. However, their approach is very memory demanding due to the high memory requirement of global volumetric representations.

Efficient multi-view stereo. Several recent works aim at reducing the cost of constructing cost volumes. Duggal *et al.* [6] prune the disparity search range during cost volume construction. Xu *et al.* [39] integrate adaptive sampling and deformable convolution into correlation-based methods [20, 17] to achieve efficient aggregation. Several other works [42, 30, 9] employ iterative refinement procedures. The above approaches either only work for pairwise rectified stereo matching tasks or have to construct a 3D cost-volume. Alternatively, Poms *et al.* [23] learn how to merge patch features for 3D reconstruction efficiently. Badki *et al.* [2] convert depth estimation as a classification task, but the resulting accuracy is not state-of-the-art. Recently, Yu *et al.* [45] proposed constructing a sparse cost-volume through regular sub-sampling and then applying Gauss-Newton iterations to refine the dense depth map. In contrast, we take an orthogonal approach to improve the efficiency based on attention-driven 2D convolutions.

Attention in 3D vision Attention mechanism has shown

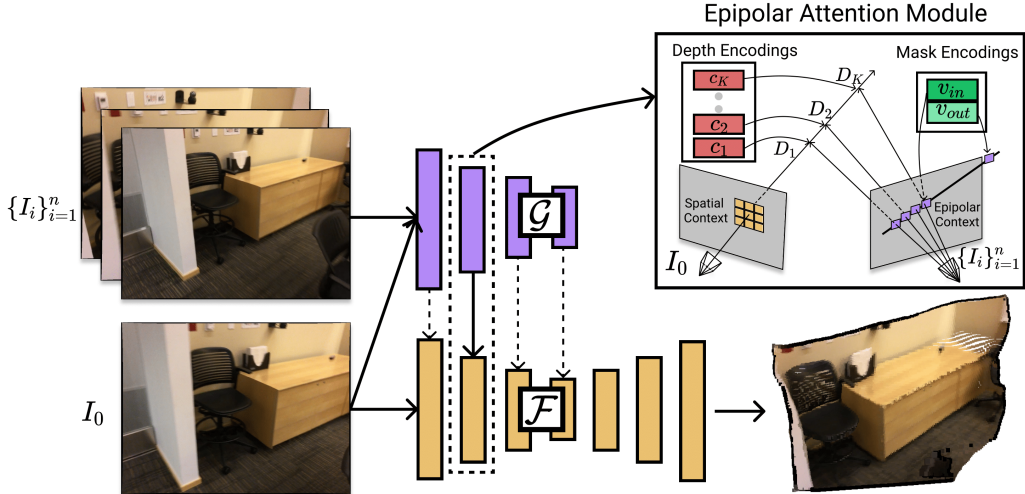


Figure 2: Network architecture of MVS2D. We employ a 2D UNet structure \mathcal{F} to make the depth prediction on I_0 , while injecting multi-view cues extracted using \mathcal{G} through the Epipolar Attention Module. Dashed arrows only exist in **Ours-robust** model (Section 3.4). We highlight that the proposed epipolar attention module can be easily integrated into most 2D CNNs.

prominent results on both natural language processing (NLP) tasks [34] and vision tasks [35]. Recently, self-local attention [25, 27] has shown promising results compared with the convolution-based counterparts. Several recent works that build an attention mechanism in MVS [19, 47, 18], but still rely on 3D CNNs and cannot avoid constructing a heavy-weighted cost volume. A promising direction is to utilize a geometry-aware 2D attention mechanism. Recent works have shown that this paradigm works well for active sensing [4, 32] and neural rendering [31]. Motivated by these works, we propose an epipolar attention module in this paper. The key contribution is a network design that aggregates single-view depth cues and multi-view depth cues to output accurate MVS outputs.

3. Approach

We provide an overview of the network architecture of MVS2D in Fig. 2. We operate in a multi-view stereo setting (Sec. 3.1), and employ a 2D UNet structure in our network design (Sec. 3.2). Our core contribution is the epipolar attention module (Sec. 3.3–3.4), which is highly accurate and efficient (Sec. 3.5) for depth estimation (Sec. 3.6).

3.1. Problem Setup

We aim to estimate the per-pixel depth for a source image $I_0 \in \mathcal{R}^{h \times w \times 3}$, given n reference images $\{I_i\}_{i=1}^n$ of the same size captured at nearby views. We assume the source image and the reference images share the same intrinsic camera matrix $\mathcal{K} \in \mathcal{R}^{3 \times 3}$, which is given. We also assume we have a good approximation of the relative camera pose between the source image and each reference image $T_i = (R_i | t_i)$, where $R_i \in \text{SO}(3)$ and $t_i \in \mathcal{R}^3$. T_i usually comes from the output of a multi-view structure-from-motion algorithm. Our goal is to recover the dense

pixel-wise depth map associated with I_0 .

We denote the homogeneous coordinate of a pixel p_0 in the source image I_0 as $\bar{p}_0 = (\bar{p}_{0,1}, \bar{p}_{0,2}, 1)^T$. Given the depth $d_0 \in \mathcal{R}$ of p_0 , the unprojected 3D point of p_0 is

$$\mathbf{p}_0(d_0) = d_0 \cdot (\mathcal{K}^{-1} \bar{p}_0).$$

Similarly, we use $\mathbf{p}_i(d_0)$ and $\bar{\mathbf{p}}_i(d_0)$ to denote respectively the 3D coordinates and homogeneous coordinates of $\mathbf{p}_0(d_0)$ in the i -th image's coordinate system. They satisfy

$$\begin{aligned} \mathbf{p}_i(d_0) &= R_i \mathbf{p}_0(d_0) + \mathbf{t}_i, \\ \bar{\mathbf{p}}_i(d_0) &= \mathcal{K} \mathbf{p}_i(d_0). \end{aligned} \quad (1)$$

3.2. Network Design Overview

In this paper, we innovate developing a multi-view stereo approach that only requires 2D convolutions. Specifically, similar to most single-view depth prediction networks, our approach progressively computes multi-scale activation maps of the source image and outputs a single depth map. The difference is that certain intermediate activation maps combine both the output of a 2D convolution operator applied to the previous activation map and the output of an attention module that aggregates multi-view depth cues. This attention module, which is the main contribution of this paper, matches each pixel of the source image and corresponding pixels on epipolar lines on the reference images. The matching procedure utilizes learned feature activations on both the source image and the reference images. The output is encoded using learned depth codes compatible with the activation maps of the source image.

Formally speaking, our goal is to learn a feed-forward network \mathcal{F} with L layers. With $\mathcal{F}_j \in \mathcal{R}^{h_j \times w_j \times m_j}$ we denote the output of the j -th layer, where m_j is its feature dimension, h_j and w_j are its height and width. Note

that the first layer $\mathcal{F}_1 \in \mathcal{R}^{h_1 \times w_1 \times 3}$ denotes the input, while the last layer $\mathcal{F}_L \in \mathcal{R}^{h_L \times w_L}$ denotes the output layer containing depth prediction. Between two consecutive layers are a general convolution operator $\mathcal{C}_j : \mathcal{R}^{h_j \times w_j \times m_j} \rightarrow \mathcal{R}^{h_j \times w_j \times m_{j+1}}$ (it can incorporate standard operators such as down-sampling, up-sampling, and max-pooling) and an optional attention module $\mathcal{A}_j : \mathcal{R}^{h_j \times w_j \times m_j} \rightarrow \mathcal{R}^{h_j \times w_j \times m_j}$:

$$\mathcal{F}_{j+1} = \mathcal{C}_j \circ \mathcal{A}_j \circ \mathcal{F}_j.$$

As we will see immediately, the attention operator \mathcal{A}_j utilizes features extracted from the reference images. Without these attention operations, \mathcal{F} becomes a standard encoder-decoder network for single-view depth prediction.

Another characteristic of this network design is that the convolution operator \mathcal{C}_j implicitly aggregates multi-view depth cues extracted at adjacent pixels. This approach promotes consistent correspondences among adjacent pixels that share the same epipolar line or have adjacent epipolar lines.

3.3. Epipolar Attention Module

We proceed to define $\mathcal{A}_j(p_0)$, which is the action of \mathcal{A}_j on each pixel p_0 . It consists of two parts:

$$\mathcal{A}_j(p_0) = \mathcal{A}_j^{\text{ep}}(p_0, \{I_i\}_{i=1}^n) + \mathcal{A}_j^0(\mathcal{F}_j(p_0)). \quad (2)$$

As we will define next, $\mathcal{A}_j^{\text{ep}}(p_0, \{I_i\}_{i=1}^n)$ uses trainable depth codes to encode the matching result between p_0 and the reference images. $\mathcal{A}_j^0 : \mathcal{R}^{m_j} \rightarrow \mathcal{R}^{m_j}$ is composed of an identity map and a trainable linear map that transforms the feature associated with p_0 in \mathcal{F}_j .

The formulation of $\mathcal{A}_j^{\text{ep}}(p_0, \{I_i\}_{i=1}^n)$ uses the *epipolar* context of p_0 . It consists of samples on the epipolar lines of p_0 on the reference images. These samples are obtained from sampling the depth values d_0 of p_0 and then applying (1). With p_i^k we denote the k -th sample on the i -th reference image.

To match p_0 and p_i^k , we introduce a feature extraction network \mathcal{G} that has identical architecture (except the attention modules) as $\mathcal{F}_{j_{\max}}$ where j_{\max} is the maximum depth of any attention module of \mathcal{F} . With $\mathcal{G}_j(I_0, p_0) \in \mathcal{R}^{m_j}$ and $\mathcal{G}_j(I_i, p_i^k) \in \mathcal{R}^{m_j}$ we denote the extracted features of p_0 and p_i^k , respectively. Following the practice of scaled-dot product attention [34], we introduce two additional trainable linear maps $f_0^j : \mathcal{R}^{m_j} \rightarrow \mathcal{R}^{m_j}$ and $f_{\text{ref}}^j : \mathcal{R}^{m_j} \rightarrow \mathcal{R}^{m_j}$ to transform the extracted features. With this setup, we define the matching score between p_0 and p_i^k as

$$w_{ik}^j = (f_0^j(\mathcal{G}_j(I_0, p_0)))^T (f_{\text{ref}}^j(\mathcal{G}_j(I_i, p_i^k))). \quad (3)$$

It remains to 1) model samples that are occluded in the reference images, and 2) bridge the weights w_{ik}^j defined in (3) and the input to the convolution operator \mathcal{C}_j . To this end, we first introduce trainable mask codes $c_{jk} \in \mathcal{R}^{m_j}$

that correspond to the k -th depth sample. We then introduce $\mathbf{v}_{\text{in}}^j \in \mathcal{R}^{m_j}$ and $\mathbf{v}_{\text{out}}^j \in \mathcal{R}^{m_j}$, which are trainable codes for inside and outside samples, respectively. Define

$$\mathbf{v}_{ik}^j = \begin{cases} \mathbf{v}_{\text{in}}^j & 0 \leq \bar{p}_{i,1}^k < w, 0 \leq \bar{p}_{i,2}^k < h, p_{i,3}^k \geq 0, \\ \mathbf{v}_{\text{out}}^j & \text{otherwise} \end{cases} \quad (4)$$

where $\bar{p}_i^k = (\bar{p}_{i,1}^k, \bar{p}_{i,2}^k, 1)^T$, $p_i^k = (p_{i,1}^k, p_{i,2}^k, p_{i,3}^k)^T$. To enhance the expressive power of \mathcal{G}_j , we further include a trainable linear map \mathcal{A}_j^1 that depends only on feature of p_0 and not on the matching results. Combing with (3) and (4), we define

$$\mathcal{A}_j^{\text{ep}}(p_0, \{I_i\}_{i=1}^n) = \mathcal{A}_j^1(\mathcal{G}_j(p_0)) + \sum_{i=1}^n \sum_{k=1}^K \mathcal{N}\left(\frac{w_{ik}^j}{\sqrt{m_j}}\right) (\mathbf{v}_{ik}^j \odot \mathbf{c}_k)) \quad (5)$$

where \mathcal{N} is the softmax normalizing function over $\frac{w_{ik}^j}{\sqrt{m_j}}$, $1 \leq k \leq K$. Substituting (5) into (2), the final attention module is given by

$$\begin{aligned} \mathcal{A}_j(p_0) = & \mathcal{A}_j^0(\mathcal{F}_j(p_0)) + \mathcal{A}_j^1(\mathcal{G}_j(p_0)) \\ & + \sum_{i=1}^n \sum_{k=1}^K \mathcal{N}\left(\frac{w_{ik}^j}{\sqrt{m_j}}\right) (\mathbf{v}_{ik}^j \odot \mathbf{c}_k)). \end{aligned}$$

Note that the attention modules at different layers have different weights.

3.4. Attention Design for Robust Multi-View Stereo

The attention mechanism above offers a rich space to design the attention modules for different inputs. Since the attention module assumes that the corresponding pixels lie on the epipolar lines, the accuracy of MVS2D depends on the relative poses' accuracy between the reference images and the source image. When input poses are accurate, our experiments suggest a single attention module at the second layer of \mathcal{F} is sufficient. This leads to a highly efficient multi-view stereo network.

When the input poses are inexact, we address this issue by installing attention modules at different resolutions of the input images, i.e., at different layers of \mathcal{F} . This approach ensures that the corresponding pixels lie sufficiently close to the epipolar lines at those resolutions at coarse resolutions. Since the convolution operations \mathcal{C}_j at different layers of \mathcal{F} aggregate multi-view features extracted at different pixels, we find this simple network design implicitly rectifies inexact epipolar lines. Figure 2 illustrates the attention modules under these two cases.

3.5. Computational Complexity

For the sake of simplicity in notation, we assume the feature channel dimension C is the same in both input and output. We denote the feature height and width as H and W respectively and denote the kernel size of convolution layers

Method	FPS (3)↑	FPS(7)↑	FPS(11)↑	Param (M)↓	AbsRel↓
Bts [16]	17.0	-	-	46.8	0.117
MVSNet [41]	4.1	2.4	1.6	1.1	0.096
DPSNet [12]	1.1	0.7	0.5	4.2	0.104
FastMVS [45]	9.0	6.0	4.3	0.4	0.089
NAS [15]	0.9	0.6	0.4	18.0	0.072
Ours-mono	94.7	-	-	12.3	0.145
Ours-robust	17.5	10.1	7.1	24.4	0.064
Ours	42.9	29.1	21.8	13.0	0.065

Table 1: Quantitative comparison on computational efficiency. FPS (V) only applies to multi-view methods [41, 45, 12, 15] and means we use V images to make the prediction. Note that numbers under the AbsRel metric are identical to those in Table 2 for ease of comparison. Please refer to section 4.4 for additional discussions.

as k . Suppose there are K depth samples, the complexity of 3D convolution is $\mathcal{O}(C^2HWKk^3)$.

For our approach, the computational complexity for executing one layer of $\mathcal{C} \circ \mathcal{A}$ is in total $\mathcal{O}(CHW(Ck^2 + K))$. Since K is usually less than Ck^2 , our module leads to a Kk times reduction in computation. The actual runtime can be found in Table 1.

3.6. Training Details

Our implementation is based on Pytorch. We optimize the smooth- l_1 loss between predicted and ground truth depth. We use Adam [14] optimizer with $\epsilon = 10^{-8}$, $\beta = (0.9, 0.999)$. We use a starting learning rate $4e^{-4}$ for ScanNet and $2e^{-4}$ for DeMoN. Please refer to supp. material for more training details.

4. Experimental Results

4.1. Datasets

ScanNet [5] The ScanNet dataset contains 807 unique scenes with image sequences captured from different camera trajectories. We sample 86324 triple images (one source image and two reference images) for training and 666 triple images for testing. Our setup ensures the scene corresponding to test images is not included in the training set.

DeMoN [33] We further validate our method on DeMoN, which is a dataset introduced by [33] for multi-view depth estimation. The training set consists of three data sources, SUN3D [37], RGBD [28], and Scenes11 [33]. SUN3D and RGBD contain real indoor scenes, while Scenes11 is synthetic. In total, there are 79577 training pairs for SUN3D, 16786 for RGBD, and 71820 for Scenes11.

4.2. Evaluation Metric

Efficiency. We benchmark our methods against baseline methods on the frame per second (FPS) during inference. We additionally compare the FPS when increasing the number of reference views.

Depth Accuracy. We use the conventional metrics of depth

estimation [16] (Table 4). Note that we do not factor out the depth scale before evaluation. The ability to correctly predict scale will render our method more applicable.

Scene Reconstruction Quality. We showcase an application of MVS2D for scene reconstruction. We follow MVSNet [41] to fuse the per-view depth map into a consistent 3D model. Please refer to supp. material for quantitative and more qualitative comparisons.

Robustness under Noisy Input Pose. We perturb the input relative poses T_j during training and report the model performance on ScanNet test set in Table 5. Please refer to the supp. material for details of the pose perturbing procedures.

4.3. Baseline Approaches

MVSNet [41] is an end-to-end plane sweeping stereo approach based on 3D-cost volume.

DPSNet [12] shares similar spirit of MVSNet [41] but focus on accurate depth map prediction.

NAS [15] is a recent work that jointly predicts consistent depth and normal, using extra normal supervision.

FastMVSNet [45] is a recent variant to MVSNet which accelerate the computation by computing sparse cost volume.

Bts [16] is a state-of-the-art single view depth prediction network. It incorporates planar priors into network design. Additionally, we use an asterisk sign '*' to denote an oracle version **Bts***, where we use the ground truth depth map to factor out the global scale.

Ours-mono is our method without the epipolar attention module, thus equivalent to single-view depth estimation. Similar to Bts*, we also report the results factoring out the global scale for **Ours-mono**.

Ours-robust is our method with multi-scale epipolar attention module applied on \mathcal{F} .

Ours is our method with epipolar attention module applied only in \mathcal{F} 's second layer.

4.4. Result Analysis

Comparison on Efficiency. We compare against both single-view methods [16] and multi-view methods [41, 45, 12, 15]. The inference speed of our method is comparable to single-view methods [16] and significantly outperforms other multi-view methods [41, 45, 12, 15]. Evaluations are done on ScanNet [5]. Our method is $48\times$ faster than NAS, $39\times$ faster than DPSNet, $10\times$ faster than MVSNet, and $4\times$ faster than the FastMVSNet. Please refer to the supp. for more details.

Comparison on Depth Estimation. MVS2D achieves considerable improvements in the depth prediction accuracy (see Table 2). On ScanNet, our approach outperforms MVSNet by large margins, reducing AbsRel error from 0.096 to 0.065. The improvements are consistent across most other metrics. Remarkably, our approach also outperforms NAS, which uses more parameters and runs 38 times slower. We visualize some depth predictions in Figure 3.

Method	AbsRel \downarrow	SqRel \downarrow	log10 \downarrow	RMSE \downarrow	RMSELog \downarrow	$\delta < 1.25 \uparrow$	$\delta < 1.25^2 \uparrow$	$\delta < 1.25^3 \uparrow$
Bts [16]	0.117	0.052	0.049	0.270	0.151	0.862	0.966	0.992
Bts* [16]	0.088	0.035	0.038	0.228	0.128	0.916	0.980	0.994
MVSNet [41]	0.096	0.051	0.043	0.299	0.147	0.882	0.969	0.991
FastMVS [45]	0.089	0.038	0.039	0.234	0.130	0.911	0.977	0.992
DPSNet [12]	0.104	0.047	0.046	0.273	0.151	0.871	0.966	0.991
NAS [15]	0.072	0.023	0.033	0.193	0.102	0.938	0.993	0.998
Ours-mono	0.145	0.065	0.061	0.300	0.173	0.807	0.957	0.990
Ours-mono*	0.103	0.037	0.044	0.237	0.135	0.892	0.984	0.996
Ours-robust	0.064	0.017	0.028	0.166	0.088	0.959	0.996	0.999
Ours	0.065	0.017	0.028	0.165	0.089	0.958	0.996	0.999

Table 2: Depth evaluation results on ScanNet [5]. We compare against both multi-view depth estimation methods [45, 41, 12, 15] and a state-of-the-art single-view method [16]. Our approach achieve 9.7% improvements over top-performing method NAS [15] on AbsRel. The improvements are consistent across all metrics.

	Method	AbsRel \downarrow	AbsDiff \downarrow	SqRel \downarrow	RMSE \downarrow	RMSELog \downarrow	$\delta < 1.25 \uparrow$	$\delta < 1.25^2 \uparrow$	$\delta < 1.25^3 \uparrow$
SUN3D (Real)	COLMAP [26]	0.623	1.327	3.236	2.316	0.661	0.327	0.554	0.718
	DeMoN [33]	0.214	2.148	1.120	2.421	0.206	0.733	0.922	0.963
	DeepMVS [11]	0.282	0.604	0.435	0.944	0.363	0.562	0.739	0.895
	DPSNet-U [12]	0.147	0.336	0.117	0.449	0.196	0.781	0.926	0.973
	NAS [15]	0.127	0.288	0.085	0.378	0.170	0.830	0.944	0.978
	Ours-robust	0.104	0.232	0.054	0.310	0.140	0.887	0.975	0.993
RGBD (Real)	COLMAP [26]	0.539	0.940	1.761	1.505	0.715	0.275	0.500	0.724
	DeMoN [33]	0.157	1.353	0.524	1.780	0.202	0.801	0.906	0.962
	DeepMVS [11]	0.294	0.621	0.430	0.869	0.351	0.549	0.805	0.922
	DPSNet-U [12]	0.151	0.531	0.251	0.695	0.242	0.804	0.895	0.927
	NAS [15]	0.131	0.474	0.213	0.619	0.209	0.857	0.929	0.945
	Ours-robust	0.088	0.315	0.151	0.428	0.148	0.924	0.946	0.957
Scenes11 (Syn)	COLMAP [26]	0.625	2.241	3.715	3.658	0.868	0.390	0.567	0.672
	DeMoN [33]	0.556	1.988	3.402	2.603	0.391	0.496	0.726	0.826
	DeepMVS [11]	0.210	0.597	0.373	0.891	0.270	0.688	0.894	0.969
	DPSNet [12]	0.050	0.152	0.111	0.466	0.116	0.961	0.982	0.988
	NAS [15]	0.038	0.113	0.067	0.371	0.095	0.975	0.990	0.995
	Ours-robust	0.063	0.183	0.149	0.576	0.141	0.967	0.984	0.989
	Ours	0.071	0.223	0.153	0.606	0.146	0.959	0.983	0.989

Table 3: Depth evaluation results on SUN3D, RGBD, and Scenes11 datasets(synthetic). The numbers for COLMAP, DeMoN, DeepMVS, DPSNet, and NAS are obtained from [15]. We achieve significant improvements on SUN3D and RGBD.

AbsRel	$\frac{1}{N} \sum_i \frac{ d_i - d_i^* }{d_i^*}$	RMSE	$\sqrt{\frac{1}{N} \sum_i (d_i - d_i^*)^2}$
SqRel	$\frac{1}{N} \sum_i \frac{(d_i - d_i^*)^2}{d_i^*}$	RMSELog	$\sqrt{\frac{1}{N} \sum_i (\log d_i - \log d_i^*)^2}$
AbsDiff	$\sqrt{\frac{1}{N} \sum_i d_i - d_i^* }$	Log10	$\frac{1}{N} \sum_i \log_{10} d_i - \log_{10} d_i^* $
$\delta < 1.25^k$	$\frac{1}{N} \sum_i (\max(\frac{d_i}{d_i^*}, \frac{d_i^*}{d_i}) < 1.25^k)$		

Table 4: Quantitative metrics for depth estimation. d_i is the predicted depth; d_i^* is the ground truth depth; N corresponds to all pixels with the ground-truth label.

Our approach yields significant improvements over single-view baselines. Adding multi-view cues improves the AbsRel of ours-mono from 0.145 to 0.065 on ScanNet. Since single-view has scale-ambiguity, we further investigate whether our methods will still be favorable when factoring out the scale. The results show that when eliminat-

ing the scale, ours-mono* has AbsRel 0.103, which is still a significant improvement. This means our approach does not simply infer the global scaling factor from multi-view cues. Compared with the single-view model, our model only incurs a 5.8% increase in parameters. Such efficiency will enable multi-view methods to embrace a much larger 2D convolutional network which is not possible before.

On other datasets, MVS2D also performs favorably (see Table 3). We achieve the AbsRel error of 0.095 on the RGBD dataset, while the next best NAS only achieves 0.131. Although MVS2D excels at adapting to the scene prior, it is encouraging that it also performs well on the Scenes11 dataset, a synthetic scene with randomly placed objects. We ranked 3rd on the Scenes11 dataset on AbsRel. Please refer to the supp. material for experiments on our

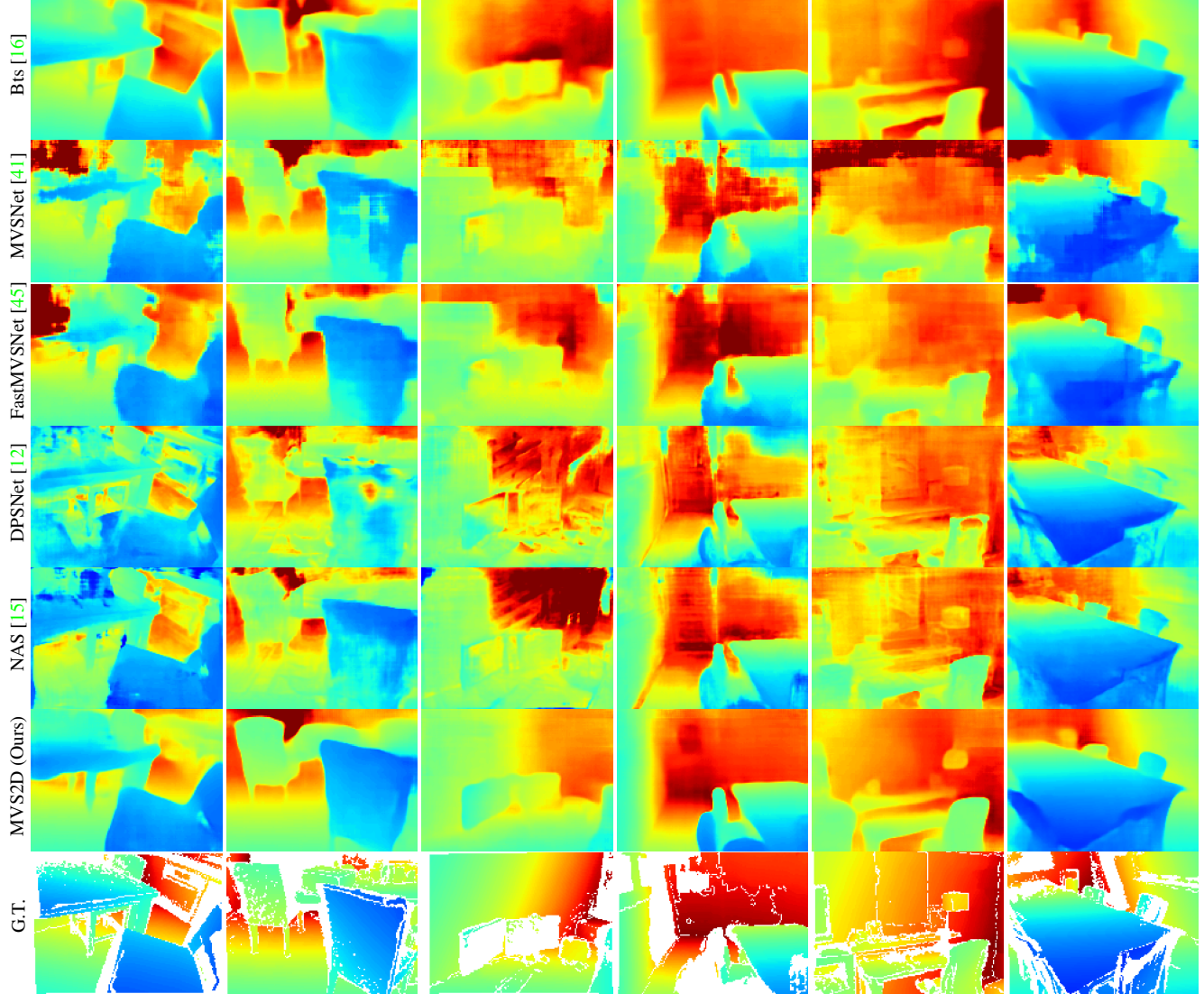


Figure 3: Qualitative results on depth prediction. Each column corresponds to one test example. The region without ground truth depth labels is colored white in the last row. Our prediction outperforms both the single-view depth estimation method [16] and other multi-view methods.

generalization ability to novel datasets.

Comparison on Dense 3D Reconstruction. We show the qualitative results of 3D reconstruction in Figure 4. Due to space limitation, we leave the all quantitative results to supp. material. Without using the cost volume, our method can achieve better results than DPSNet and NAS. Our approach is also comparable to MVSNet & FastMVSNet, which are designed for 3D reconstruction. Qualitatively, we found our reconstruction is less noisy on flat surface areas. The behavior is reasonable because our approach utilizes strong single-view priors.

Comparison on Robustness under Noisy Pose. As shown in Table 2, Ours-robust (multi-scale cues) and Ours (single-scale cues) perform similarly when the input poses are ac-

curate. However, as shown in Table 5, multi-scale aggregation is preferred when the input poses are noisy. It suggests that when having inaccurate training data, it is necessary to incorporate multi-scale cues, though at a cost of increased computations (as shown in Table 1).

Ablation Study on Depth Encoding. The ablation study of our depth code design can be found in Table 6. We tested four code types. ‘Uniform’ serves as a sanity check, where we use the same code vector for all depth hypotheses. In other words, the network does not extract useful information from the reference images. ‘Linear’ improves on uniform encoding by scaling a base code vector with the corresponding depth value. ‘Cosine’ codes are identical to the one used in [34]. ‘Learned’ codes are optimized end-to-end.

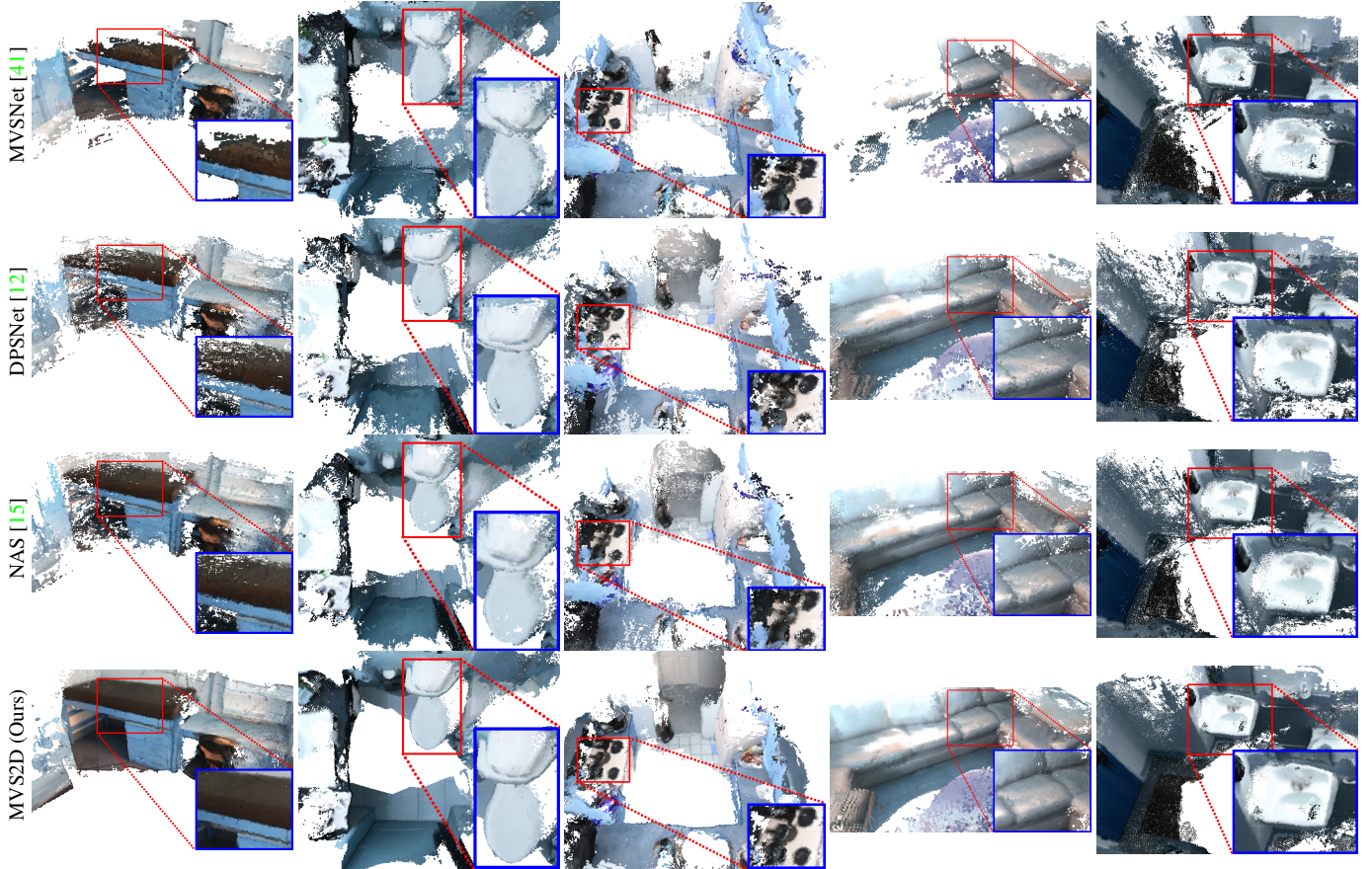


Figure 4: Qualitative scene reconstruction results on ScanNet. Our method yields smoother outputs than other baselines. We zoom in parts of a scene (red box) and show at the corner (blue box) to highlight the differences. Best viewed in PDF.

Metric	MVSNet	DPSNet	Ours	Ours-robust
AbsRel \downarrow	0.096	0.104	0.065	0.064
AbsRel (p) \downarrow	0.118	0.135	0.082	0.075
$\Delta \downarrow$	0.022	0.031	0.017	0.011
$\delta < 1.25 \uparrow$	0.882	0.871	0.958	0.959
$\delta < 1.25$ (p) \uparrow	0.838	0.802	0.939	0.944
$\Delta \downarrow$	0.044	0.069	0.019	0.015

Table 5: Different methods’ performance under noisy input poses on ScanNet [5]. We notice that most methods suffer from significant performance drops. Our method with multi-scale epipolar aggregation shows notable robustness.

We can see that learning the codes end-to-end leads to noticeable performance gains. One explanation is that these learned codes can adapt to the single-view feature representations of the source image.

5. Conclusions

We proposed a simple yet effective method for multi-view stereo. The core of our method is to integrate single-view and multi-view cues during the prediction jointly. Such a design not only improves the performance but also

Metric	Uniform	Linear	Cosine	Learned
AbsRel \downarrow	0.152	0.116	0.070	0.065
$\delta < 1.25 \uparrow$	0.795	0.869	0.954	0.958
RMSE \downarrow	0.310	0.265	0.172	0.165

Table 6: Ablation study on different depth encodings.

has the appealing factor of being efficient. Furthermore, we have demonstrated the trade-off between input pose accuracy and network complexity. When the input pose is exact, we can leverage minimum additional computation to inject the multi-view information. Our approach opens doors for using 2D CNNs for fast multi-view stereo.

One potential direction is instead of using a fixed number of depth samples, learn to place a spatially varying number of samples to further increase efficiency.

Acknowledgements. Qixing Huang would like to acknowledge the support from NSF IIS-2047677 and NSF HDR TRIPODS-1934932.

References

[1] Henrik Aanæs, Rasmus Ramsbøl Jensen, George Vogiatzis, Engin Tola, and Anders Bjorholm Dahl. Large-scale data for multiple-view stereopsis. *International Journal of Computer Vision (IJCV)*, 120(2):153–168, 2016. 2

[2] Abhishek Badki, Alejandro Troccoli, Kihwan Kim, Jan Kautz, Pradeep Sen, and Orazio Gallo. Bi3D: Stereo depth estimation via binary classifications. In *Proceedings of the IEEE Conference on Computer Vision and Pattern Recognition (CVPR)*, pages 1600–1608, 2020. 2

[3] Rui Chen, Songfang Han, Jing Xu, and Hao Su. Point-based multi-view stereo network. In *Proceedings of the IEEE International Conference on Computer Vision (ICCV)*, pages 1538–1547, 2019. 2

[4] Ricson Cheng, Ziyan Wang, and Katerina Fragkiadaki. Geometry-aware recurrent neural networks for active visual recognition. In *Advances in Neural Information Processing Systems (NeurIPS)*, pages 5086–5096, 2018. 3

[5] Angela Dai, Angel X. Chang, Manolis Savva, Maciej Halber, Thomas Funkhouser, and Matthias Nießner. ScanNet: Richly-annotated 3D reconstructions of indoor scenes. In *Proceedings of the IEEE Conference on Computer Vision and Pattern Recognition (CVPR)*, 2017. 1, 2, 5, 6, 8

[6] Shivam Duggal, Shenlong Wang, Wei-Chiu Ma, Rui Hu, and Raquel Urtasun. DeepPruner: Learning efficient stereo matching via differentiable patchmatch. In *Proceedings of the IEEE International Conference on Computer Vision (ICCV)*, pages 4384–4393, 2019. 2

[7] Yasutaka Furukawa and Carlos Hernández. Multi-view stereo: A tutorial. *Found. Trends. Comput. Graph. Vis.*, 9(1–2):1–148, June 2015. 1, 2

[8] Yasutaka Furukawa and Jean Ponce. Accurate camera calibration from multi-view stereo and bundle adjustment. *International Journal of Computer Vision (IJCV)*, 84(3):257–268, 2009. 2

[9] Xiaodong Gu, Zhiwen Fan, Siyu Zhu, Zuozhuo Dai, Feitong Tan, and Ping Tan. Cascade cost volume for high-resolution multi-view stereo and stereo matching. In *Proceedings of the IEEE Conference on Computer Vision and Pattern Recognition (CVPR)*, pages 2495–2504, 2020. 1, 2

[10] Asmaa Hosni, Christoph Rhemann, Michael Bleyer, Carsten Rother, and Margrit Gelautz. Fast cost-volume filtering for visual correspondence and beyond. *IEEE Transactions on Pattern Analysis and Machine Intelligence (TPAMI)*, 35(2):504–511, 2012. 2

[11] Po-Han Huang, Kevin Matzen, Johannes Kopf, Narendra Ahuja, and Jia-Bin Huang. DeepMVS: Learning multi-view stereopsis. In *Proceedings of the IEEE Conference on Computer Vision and Pattern Recognition (CVPR)*, pages 2821–2830, 2018. 1, 2, 6

[12] Sunghoon Im, Hae-Gon Jeon, Stephen Lin, and In So Kweon. DPSNet: End-to-end deep plane sweep stereo. In *International Conference on Learning Representations (ICLR)*, 2019. 1, 2, 5, 6, 7, 8

[13] Abhishek Kar, Christian Häne, and Jitendra Malik. Learning a multi-view stereo machine. In *Advances in Neural Information Processing Systems (NeurIPS)*, pages 364–375, 2017. 2

[14] Diederik P. Kingma and Jimmy Ba. Adam: A method for stochastic optimization. In Yoshua Bengio and Yann LeCun, editors, *International Conference on Learning Representations (ICLR)*, 2015. 5

[15] Uday Kusupati, Shuo Cheng, Rui Chen, and Hao Su. Normal assisted stereo depth estimation. *Proceedings of the IEEE Conference on Computer Vision and Pattern Recognition (CVPR)*, 2020. 1, 2, 5, 6, 7, 8

[16] Jin Han Lee, Myung-Kyu Han, Dong Wook Ko, and Il Hong Suh. From big to small: Multi-scale local planar guidance for monocular depth estimation. *arXiv preprint arXiv:1907.10326*, 2019. 1, 5, 6, 7

[17] Zhengfa Liang, Yiliu Feng, Yulan Guo, Hengzhu Liu, Wei Chen, Linbo Qiao, Li Zhou, and Jianfeng Zhang. Learning for disparity estimation through feature constancy. In *Proceedings of the IEEE Conference on Computer Vision and Pattern Recognition (CVPR)*, pages 2811–2820, 2018. 1, 2

[18] Xiaoxiao Long, Lingjie Liu, Wei Li, Christian Theobalt, and Wenping Wang. Multi-view depth estimation using epipolar spatio-temporal networks. In *Proceedings of the IEEE Conference on Computer Vision and Pattern Recognition (CVPR)*, 2021. 2, 3

[19] Keyang Luo, Tao Guan, Lili Ju, Yuesong Wang, Zhuo Chen, and Yawei Luo. Attention-aware multi-view stereo. In *Proceedings of the IEEE Conference on Computer Vision and Pattern Recognition (CVPR)*, pages 1590–1599, 2020. 3

[20] Nikolaus Mayer, Eddy Ilg, Philip Hausser, Philipp Fischer, Daniel Cremers, Alexey Dosovitskiy, and Thomas Brox. A large dataset to train convolutional networks for disparity, optical flow, and scene flow estimation. In *Proceedings of the IEEE Conference on Computer Vision and Pattern Recognition (CVPR)*, pages 4040–4048, 2016. 1, 2

[21] Zak Murez, Tarrence van As, James Bartolozzi, Ayan Sinha, Vijay Badrinarayanan, and Andrew Rabinovich. Atlas: End-to-end 3D scene reconstruction from posed images. In *Proceedings of the European Conference on Computer Vision (ECCV)*, 2020. 1, 2

[22] Guang-Yu Nie, Ming-Ming Cheng, Yun Liu, Zhengfa Liang, Deng-Ping Fan, Yue Liu, and Yongtian Wang. Multi-level context ultra-aggregation for stereo matching. In *Proceedings of the IEEE Conference on Computer Vision and Pattern Recognition (CVPR)*, pages 3283–3291, 2019. 1, 2

[23] Alex Poms, Chenglei Wu, Shou-I Yu, and Yaser Sheikh. Learning patch reconstructability for accelerating multi-view stereo. In *Proceedings of the IEEE Conference on Computer Vision and Pattern Recognition (CVPR)*, pages 3041–3050, 2018. 2

[24] Xiaojuan Qi, Renjie Liao, Zhengzhe Liu, Raquel Urtasun, and Jiaya Jia. Geonet: Geometric neural network for joint depth and surface normal estimation. In *Proceedings of the IEEE Conference on Computer Vision and Pattern Recognition (CVPR)*, pages 283–291, 2018. 1

[25] Prajit Ramachandran, Niki Parmar, Ashish Vaswani, Irwan Bello, Anselm Levskaya, and Jonathon Shlens. Stand-alone self-attention in vision models. *Advances in Neural Information Processing Systems (NeurIPS)*, 2019. 3

[26] Johannes L. Schönberger and Jan-Michael Frahm. Structure-from-motion revisited. In *Proceedings of the IEEE Conference on Computer Vision and Pattern Recognition (CVPR)*, pages 4104–4113, 2016. 6

[27] Peter Shaw, Jakob Uszkoreit, and Ashish Vaswani. Self-attention with relative position representations. In *Proceedings of the 2018 Conference of the North American Chapter of the Association for Computational Linguistics: Human Language Technologies, Volume 2 (Short Papers)*, pages 464–468, 2018. 3

[28] J. Sturm, N. Engelhard, F. Endres, W. Burgard, and D. Cremers. A benchmark for the evaluation of RGB-D SLAM systems. In *IEEE/RSJ International Conference on Intelligent Robots and Systems (IROS)*, 2012. 2, 5

[29] Deqing Sun, Xiaodong Yang, Ming-Yu Liu, and Jan Kautz. PWC-Net: CNNs for optical flow using pyramid, warping, and cost volume. In *Proceedings of the IEEE Conference on Computer Vision and Pattern Recognition (CVPR)*, pages 8934–8943, 2018. 2

[30] Vladimir Tankovich, Christian Häne, Sean Fanello, Yinda Zhang, Shahram Izadi, and Sofien Bouaziz. HITNet: Hierarchical iterative tile refinement network for real-time stereo matching. *arXiv preprint arXiv:2007.12140*, 2020. 2

[31] Josh Tobin, OpenAI Robotics, and Pieter Abbeel. Geometry-aware neural rendering. *Advances in Neural Information Processing Systems (NeurIPS)*, 2019. 3

[32] Hsiao-Yu Fish Tung, Ricson Cheng, and Katerina Fragkiadaki. Learning spatial common sense with geometry-aware recurrent networks. In *Proceedings of the IEEE Conference on Computer Vision and Pattern Recognition (CVPR)*, pages 2595–2603, 2019. 3

[33] Benjamin Ummenhofer, Huizhong Zhou, Jonas Uhrig, Niklaus Mayer, Eddy Ilg, Alexey Dosovitskiy, and Thomas Brox. Demon: Depth and motion network for learning monocular stereo. In *Proceedings of the IEEE Conference on Computer Vision and Pattern Recognition (CVPR)*, pages 5622–5631, 2017. 2, 5, 6

[34] Ashish Vaswani, Noam Shazeer, Niki Parmar, Jakob Uszkoreit, Llion Jones, Aidan N Gomez, Łukasz Kaiser, and Illia Polosukhin. Attention is all you need. *Advances in Neural Information Processing Systems (NeurIPS)*, 2017. 3, 4, 7

[35] Xiaolong Wang, Ross Girshick, Abhinav Gupta, and Kaiming He. Non-local neural networks. In *Proceedings of the IEEE Conference on Computer Vision and Pattern Recognition (CVPR)*, pages 7794–7803, 2018. 3

[36] Yuesong Wang, Tao Guan, Zhuo Chen, Yawei Luo, Keyang Luo, and Lili Ju. Mesh-guided multi-view stereo with pyramid architecture. In *Proceedings of the IEEE Conference on Computer Vision and Pattern Recognition (CVPR)*, pages 2039–2048, 2020. 2

[37] Jianxiong Xiao, Andrew Owens, and Antonio Torralba. SUN3D: A database of big spaces reconstructed using sfm and object labels. In *Proceedings of the IEEE International Conference on Computer Vision (ICCV)*, pages 1625–1632, 2013. 1, 2, 5

[38] Dan Xu, Elisa Ricci, Wanli Ouyang, Xiaogang Wang, and Nicu Sebe. Multi-scale continuous CRFs as sequential deep networks for monocular depth estimation. In *Proceedings of the IEEE Conference on Computer Vision and Pattern Recognition (CVPR)*, 2017. 1

[39] Haofei Xu and Juyong Zhang. AANet: Adaptive aggregation network for efficient stereo matching. In *Proceedings of the IEEE Conference on Computer Vision and Pattern Recognition (CVPR)*, pages 1959–1968, 2020. 2

[40] Zhenpei Yang, Li Erran Li, and Qixing Huang. Strumonet: Structure-aware monocular 3d prediction. In *Proceedings of the IEEE Conference on Computer Vision and Pattern Recognition (CVPR)*, 2021. 1

[41] Yao Yao, Zixin Luo, Shiwei Li, Tian Fang, and Long Quan. Mvsnet: Depth inference for unstructured multi-view stereo. In *Proceedings of the European Conference on Computer Vision (ECCV)*, pages 767–783, 2018. 1, 2, 5, 6, 7, 8

[42] Yao Yao, Zixin Luo, Shiwei Li, Tianwei Shen, Tian Fang, and Long Quan. Recurrent MVSNet for high-resolution multi-view stereo depth inference. In *Proceedings of the IEEE Conference on Computer Vision and Pattern Recognition (CVPR)*, pages 5525–5534, 2019. 1, 2

[43] Yao Yao, Zixin Luo, Shiwei Li, Jingyang Zhang, Yufan Ren, Lei Zhou, Tian Fang, and Long Quan. Blendedmvs: A large-scale dataset for generalized multi-view stereo networks. *Proceedings of the IEEE Conference on Computer Vision and Pattern Recognition (CVPR)*, 2020. 2

[44] Wei Yin, Yifan Liu, Chunhua Shen, and Youliang Yan. Enforcing geometric constraints of virtual normal for depth prediction. In *Proceedings of the IEEE International Conference on Computer Vision (ICCV)*, pages 5684–5693, 2019. 1

[45] Zehao Yu and Shenghua Gao. Fast-MVSNet: Sparse-to-dense multi-view stereo with learned propagation and gauss-newton refinement. In *Proceedings of the IEEE Conference on Computer Vision and Pattern Recognition (CVPR)*, pages 1949–1958, 2020. 1, 2, 5, 6, 7

[46] Jure Zbontar and Yann LeCun. Computing the stereo matching cost with a convolutional neural network. In *Proceedings of the IEEE Conference on Computer Vision and Pattern Recognition (CVPR)*, pages 1592–1599, 2015. 2

[47] Xudong Zhang, Yutao Hu, Haochen Wang, Xianbin Cao, and Baochang Zhang. Long-range attention network for multi-view stereo. In *IEEE Winter Conference on Applications of Computer Vision (WACV)*, pages 3782–3791, 2021. 3